Coupled optical resonance laser locking

S. C. Burd,[1,2,*] **P. J. W. du Toit,**[1,3] **and H. Uys**[1,4]

[1]*National Laser Centre, Council for Scientific and Industrial Research Brummeria, Pretoria, Gauteng, 0184, South Africa*
[2]*School of Physics and Chemistry, University of KwaZulu-Natal Durban 4041, South Africa*
[3]*Department of Physics, University of Pretoria, Pretoria 0028, South Africa*
[4]*huys@csir.co.za*

[*]*shaun.burd@colorado.edu*

Abstract: We have demonstrated simultaneous laser frequency stabilization of a UV and IR laser, to coupled transitions of ions in the same spectroscopic sample, by detecting only the absorption of the UV laser. Separate signals for locking the different lasers are obtained by modulating each laser at a different frequency and using lock-in detection of a single photodiode signal. Experimentally, we simultaneously lock a 369nm and a 935nm laser to the $^2S_{1/2} \rightarrow {}^2P_{1/2}$ and $^2D_{3/2} \rightarrow {}^3D_{[3/2]1/2}$ transitions, respectively, of Yb^+ ions generated in a hollow cathode discharge lamp. Stabilized lasers at these frequencies are required for cooling and trapping Yb^+ ions, used in quantum information and in high precision metrology experiments. This technique should be readily applicable to other ion and neutral atom systems requiring multiple stabilized lasers.

OCIS codes: (020.0020) Atomic and molecular physics; (120.0120) Instrumentation, measurement, and metrology; (270.0270) Quantum optics; (300.0300) Spectroscopy; (140.0140) Lasers and laser optics; (140.3425) Laser stabilization.

References and links

1. H. J. Metcalf and P. van der Straten, *Laser Cooling and Trapping* (Springer, 1999).
2. E. Streed, T. Weinhold, and D. Kielpinski, "Frequency stabilization of an ultraviolet laser to ions in a discharge," Appl. Phys. Lett. **93**, 071103 (2008).
3. M. W. Lee, M. C. Jarratt, C. Marciniak, and M. J. Biercuk, "Frequency stabilization of a 369 nm diode laser by nonlinear spectroscopy of ytterbium ions in a discharge," Opt. Express **22**(6), 7210–7221 (2014).
4. J. J. McLoughlin, A. H. Nizamani, J. D. Siverns, R. C. Sterling, M. D. Hughes, B. Lekitsch, B. Stein, S. Weidt, and W. K. Hensinger, "Versatile ytterbium ion trap experiment for operation of scalable ion-trap chips with motional heating and transition-frequency measurements," Phys. Rev. A **83**, 013406 (2011).
5. S. Olmschenk, K. C. Younge, D. L. Moehring, D. N. Matsukevich, P. Maunz, and C. Monroe, "Manipulation and detection of a trapped Yb^+ hyperfine qubit," Phys. Rev. A **76**, 052314 (2007).
6. H. S. Moon, W. K. Lee, L. Lee, and J. Kim, "Double resonance optical pumping spectrum and its application for frequency stabilization of a laser diode," Appl. Phys. Lett. **76**(18), 3965–3967 (2004).
7. F. E. Becerra, R. T. Willes, S. R. Rolston, and L. A. Orozco, "Two-photon dichroic atomic vapor laser lock using electromagnetically induced transparency and absorption," J. Opt. Soc. Am. B. **26**(7), 1315–1320 (2009).
8. A. Perez Galvan, D. Sheng, L. A. Orozco, and Y. Zhao, "Two-color modulation transfer spectroscopy," Can. J. Phys. **87**, 95–100 (2009).
9. M. Petrasiunas, E. W. Streed, T. Weinhold, B. Norton, and D. Kielpinski, "Optogalvanic spectroscopy of metastable states in Yb^+," Appl. Phys. B **107**(4), 1053–1059 (2012).
10. A. M. Märtensson-Pendril, D. S.Gough and P. Hannaford, "Isotope shifts and hyperfine structure in the 369.4-nm $^6s_{1/2}$-$^6p_{1/2}$ resonance line of singly ionized ytterbium," Phys. Rev. A **49**, 3351–3365 (1994).
11. A. T. Nguyen, L. B. Wang, M. M. Schauer and J. R. Torgerson, "Extended temperature tuning of an ultraviolet diode laser for trapping and cooling single Yb^+ ions," Rev. Sci. Instr. **81**, 053110 (2010).
12. P. W. Smith and T. Hänsch, "Cross relaxation effects in the saturation of the 6328 neon-laser line," Phys. Rev. Lett. **26**, 740–743 (1971).

#217611 - $15.00 USD Received 23 Jul 2014; revised 29 Aug 2014; accepted 1 Sep 2014; published 7 Oct 2014

13. J. Tenenbaum, E. Miron, S. Lavi, J. Liran, M Strauss, J. Oreg, and G. Erez, "Velocity changing collisions in saturation absorption of U," J. Phys. B **16**, 4543–4553 (1983).
14. W. Demtroder, *Laser Spectroscopy*, 4th ed. (Springer, 2008), Vol I.
15. J. H. Shirley, "Modulation transfer processes in optical heterodyne saturation spectroscopy," Opt. Lett. **7**(11), 537–539 (1982).
16. J. F. Eble and F. Schmid-Kaler, "Optimization of frequency modulation transfer spectroscopy on the calcium 4^1s_0 to 4^1p_1 transition," Appl. Phys. B **88**(4), 563–568 (2007).
17. D. J. McCarron, S. A. King, and S. L. Cornish, "Modulation transfer spectroscopy in atomic rubidium," Meas. Sci. Technol **19**(10), 105601 (2008).

1. Introduction

Frequency stabilized lasers are an integral part of many atomic physics experiments. Particularly in trapped ion or neutral atom experiments, the laser frequency must be stabilized to be within a fraction of the natural line width of an atomic transition for effective cooling and state manipulation [1]. Additional stabilized lasers are generally required to prevent shelving of the ion in metastable states to ensure high scattering rates on the primary cooling transition or to deliberately shelve the ion in a specific state.

Traditionally, lasers in the visible or infrared have been locked to molecular or atomic vapour cells using standard spectroscopic techniques. The stabilized laser frequency will generally need to be shifted using external acousto- or electro-optical modulation to be sufficiently close to the resonance of interest of the trapped ion. The need for this shift can be reduced or eliminated by using atoms of the same species in the vapour cell as the atoms that are to be trapped. Alkali metal vapour cells are frequently used as references for neutral atom experiments involving these metals. Streed et al. [2] and Lee at al. [3] have demonstrated locking a UV diode laser to the $^2S_{1/2} \rightarrow {}^2P_{1/2}$ transition of Yb^+ ions generated in a hollow cathode discharge lamp. Generally, these techniques do not provide a method for locking to a metastable state transition. The challenge arises when the lower lying state of a metastable spectroscopic transition is only weakly populated, and scattering on the transition is dominated by Raman decay to other levels. This leads to the absence of a significant absorption signal for stabilizing the laser. To address this, an option is to use one spectroscopically stabilized laser as a reference, and to lock additional lasers by using a Fabry Perot cavity to measure the relative frequencies between the lasers [4, 5].

Here we present an alternative method of meeting this challenge by locking two lasers to coupled resonances of ions which we call Coupled Optical REsonance Laser Locking, or CORELL. By allowing lasers with different wavelengths to propagate collinearly and interact resonantly with coupled transitions of the same ions, we can obtain separate signals suitable for locking each laser, even though the absorption of only one of the lasers is observed. We demonstrate the technique experimentally for Yb^+ ions in a hollow cathode discharge lamp (HCDL). The spectroscopic technique used in our method is reminiscent of double resonance spectroscopy, usually employed in a three level ladder structure [6–8]. It is however, distinct in that the two lasers address two transitions in a four level structure that do not share a common level, and are coupled only through spontaneous decay.

Figure 1 shows the relevant energy levels of the cooling and main re-pumping transitions of $^{174}Yb^+$ for ion trap experiments. The $^2S_{1/2} \rightarrow {}^2P_{1/2}$ cooling transition has a UV center wavelength at 369.525nm. This cooling cycle is not completely closed due to a spontaneous emission branching ratio of 0.005, from the $^2P_{1/2}$ to the metastable $^2D_{3/2}$ state [5]. A trapped ion that falls into the metastable $^2D_{3/2}$ state will no longer be able to scatter photons from the cooling beam. To return the ion to the cooling cycle an IR laser at 935.180nm is used to excite ions from the $^2D_{3/2}$ state to the $^3D[3/2]_{1/2}$ state, where they rapidly decay back to the $^2S_{1/2}$ ground state with 0.982 probability. This efficient decay strongly suppresses any absorption signal due

#217611 - $15.00 USD Received 23 Jul 2014; revised 29 Aug 2014; accepted 1 Sep 2014; published 7 Oct 2014

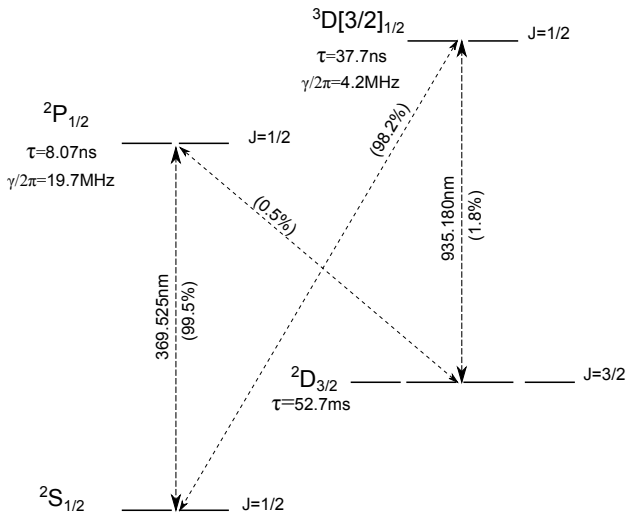

Fig. 1. Energy levels of $^{174}Yb^+$. Spontaneous emission branching ratios are indicated in brackets.

to the 935 nm laser alone, since the scattering does not cycle on the $^2\mathrm{D}_{3/2} \rightarrow ^3\mathrm{D}[3/2]_{1/2}$ transition. Absorption of the 935 nm laser is further suppressed because, without optical pumping, only few ions in the electric discharge of our HCDL will be in the $^2D_{3/2}$ state [9]. These effects conspire to make observation of absorption of the 935 nm laser very challenging, thus precluding the use of conventional techniques like saturated absorption spectroscopy for stabilizing its frequency. The coupled resonance technique discussed here overcomes this obstacle, and works as follows.

If the $^2\mathrm{S}_{1/2} \rightarrow {}^2\mathrm{P}_{1/2}$ transition is driven at resonance, there will be a net increase of ions in the $^2\mathrm{D}_{3/2}$ state and a decrease in the population of ions in the ground state. If the 935nm laser is then tuned to the $^2\mathrm{D}_{3/2} \rightarrow {}^3\mathrm{D}[3/2]_{1/2}$ transition, the metastable state will be depleted and the $^2\mathrm{S}_{1/2}$ state will be repopulated. Thus the 935nm laser will affect the population of the $^2\mathrm{S}_{1/2}$ ground state. The effective lifetime for decay from $^2\mathrm{P}_{1/2}$ into the $^3\mathrm{D}[3/2]_{1/2}$ state is $\tau_{eff} = 8.07\mathrm{ns}/0.005 = 1.6\mu\mathrm{s}$. The rate of population transfer to the $^2D_{3/2}$ state is therefore 3.3×10^4 greater than the rate of decay of the metastable state directly back to the $^2\mathrm{S}_{1/2}$ state via spontaneous emission along the $^2D_{3/2} \rightarrow {}^2\mathrm{S}_{1/2}$ transition. This large flow of ions into the $^2\mathrm{D}_{3/2}$ state can cause an observable change in the absorption of the 369nm laser. The effect of the separate lasers can be observed with lock-in detection by monitoring the saturated absorption signal of the 369nm laser and modulating each laser at a different frequency. For laser frequency stabilization, the line center of the 369nm transition is detected using a phase modulation technique. Once the 369nm laser is locked to the line center, tuning the 935nm laser through the $^2\mathrm{D}_{3/2} \rightarrow {}^3\mathrm{D}[3/2]_{1/2}$ resonance will generate an error signal suitable for stabilizing the 935nm laser.

In what follows, we first describe the observation of the coupled optical resonance spectroscopy signals. In order to elucidate the underlying physics we then develop a four-level rate equation model incorporating velocity changing collisions. We end by demonstrating simultaneous frequency stabilization of the UV an IR lasers using CORELL.

#217611 - $15.00 USD Received 23 Jul 2014; revised 29 Aug 2014; accepted 1 Sep 2014; published 7 Oct 2014

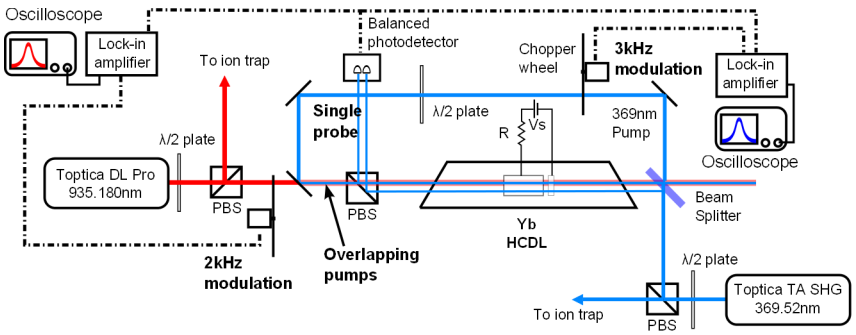

Fig. 2. Optical layout for CORELL spectroscopy. HCDL - Hollow Cathode Discharge Lamp, PID - Proportional-Integral-Differential controller, PBS - polarization Beam Splitter. The lamp voltage V_s is typically kept at 630V, and R is a ballast resitor.

2. Coupled resonance spectroscopy of Yb^+ ions

The experimental setup used to perform coupled resonance spectroscopy is shown in Fig. 2. 369.525nm light is generated by frequency doubling an amplified external cavity 739.050nm diode laser (Toptica Photonics TA-SHG). The 935nm beam is generated using an external cavity diode laser (Toptica Photonics DL PRO). The 369nm beam is split into a strong pump beam and two weak probe and reference beams by passing it through a 4% beam sampler. The pump and probe beams counter-propagate through an Yb HCDL (Hamamatsu L2783-70NE-Yb). The pump beam is made to overlap with the probe beam, while the second weak beam is used as an unsaturating reference to reduce intensity noise and subtract the Doppler background in saturated absorption experiments. After passing through the lamp, the two probe beams are directed to a balanced photodetector. To improve the signal to noise ratio, the 369nm pump beam is chopped at 3kHz and a lock-in amplifier is used to filter and amplify the signal from the balanced photodetector. The 935nm beam propagates collinearly with the 369nm pump beam. The two beams are combined with a beam splitter.

The 935nm spectroscopic signal is also contained in the output signal of the balanced photodetector which only monitors the intensity of the 369nm probe beams. The photodetector signal is also used as the input to a second lock-in amplifier. The 935nm beam is modulated at a different frequency from the 369nm laser. The wavelengths of the lasers are monitored with a Bristol Model 621 wavelength meter.

To observe the hyperfine structure of the $^2S_{1/2} \rightarrow ^2P_{1/2}$ transition of the Yb^+ isotopes in the HCDL, the wavelength of the 369nm laser is scanned from 369.521nm to 369.527nm by adjusting the grating of the 739nm master laser. The spectrum obtained by referencing to the frequency at which the 369nm beam is chopped is shown as the blue curve in Fig. 3. A pump beam power of 10mW and probe power of 0.45mW were used. The beam waist at the lamp center is 0.4mm (measured). Note that the widths of the 369nm Doppler-free features are larger than the natural line width (19.2MHz) due to power and pressure broadening mechanisms. Precise resonant frequencies for the different ytterbium isotopes for the 369nm transition have been measured by McLoughlin et al. [4] who used trapped ions as a reference. These values correspond closely with the measured wavelengths of resonance peaks in the saturated absorption spectrum in Fig. 3, and were used to identify the isotopes. The spectrum is also in good agreement with that obtained by Märtensson-Pendrill et al. [10], and Nguyen et al. [11].

When the 935nm laser, on resonance with the $^2D_{3/2} \rightarrow ^3D[3/2]_{1/2}$ transition of a given iso-

#217611 - $15.00 USD Received 23 Jul 2014; revised 29 Aug 2014; accepted 1 Sep 2014; published 7 Oct 2014

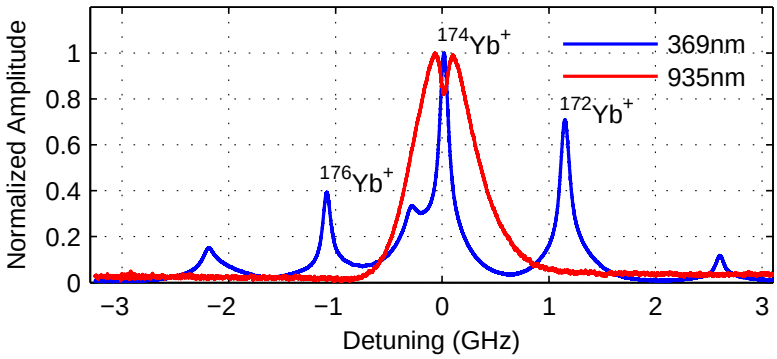

Fig. 3. Experimental spectroscopic signals obtained by scanning the 369nm laser frequency and holding the 935nm laser on resonance for the repump transition of $^{174}Yb^{+}$. The signal from the lock-in amplifier referenced to the modulation frequency of the 369nm pump is shown in blue. The signal from the lock-in amplifier referenced to the modulation frequency of the 935nm laser is shown in red. Both signals are independently normalized. Note that the blue curve is due to increased *transmission* of the 369nm laser probe, due to saturation. On the other hand, the red curve is due to increased *absorption* of the 369nm laser due to re-population of the $2S_{1/2}$ state by the 935nm laser. The full-width half-maximum of the 935nm feature is 683MHz, while that of the $^{174}Yb^{+}$ saturation feature at 369nm is 160MHz. A lock-in time constant of 3ms was used, and the graph shows the average over 16 oscilloscope traces.

tope, interacts with the ions in the lamp, and the 369nm laser is scanned over the $^2S_{1/2} \rightarrow {}^2P_{1/2}$ transition of the same isotope, ions in the $^2D_{3/2}$ state will be transferred to the $2S_{1/2}$ state and there will be increased absorption of 369nm photons. Lock-in detection of the photodetector signal, referenced to the modulation frequency of the 935nm laser, produces an output signal of a broadened peak with a prominent central dip, shown as the red curve in Fig. 3. Here 8.5mW of 935nm light (beam radius 0.4mm) was focused through the lamp and overlapped with the 369nm pump. Observe that the center of the signal due to the 935nm laser occurs exactly at the center of the $^2S_{1/2} \rightarrow {}^2P_{1/2}$ transition of $^{174}Yb^{+}$, and that no features appear for any of the other isotopes. It is important to note that if the frequency of the 935nm laser is slightly detuned from resonance, the magnitude and signal-to-noise ratio of the signal will reduce, but the center of the feature will still correspond to the peak of the 369nm resonance. The signal is a measure of the change in the absorption of the 369nm laser due to the re-population of the $^2S_{1/2}$ state by the 935nm laser. In Fig. 3 both signals are independently normalized, but we estimate that the raw signal inputs to the lock-in amplifiers, referenced to the modulation frequencies of the 369nm versus 935nm pump beams, have a ratio of 200:1.

In Fig. 4(a), we map the experimental coupled resonance topology as a function of the detuning of both lasers. The plot exhibits an asymmetry, which is a result of velocity dependent population depletion of the $^2D_{3/2}$ state by the detuned 935nm laser. Red (blue) detuning of the 935nm laser will selectively repump ions moving towards (away from) the source which can then absorb blue (red) detuned 369nm probe photons since the probe travels in the opposite direction through the lamp. Observe that if the 369nm laser field is at zero detuning, scanning the 935nm laser results in a feature symmetric about the 935nm resonance.

These results can be understood using a four-level population state model where the steady state populations of all levels in the system are calculated as a function of the frequencies of both lasers. The populations are then used to calculate the relative absorption signal of the single

#217611 - $15.00 USD Received 23 Jul 2014; revised 29 Aug 2014; accepted 1 Sep 2014; published 7 Oct 2014

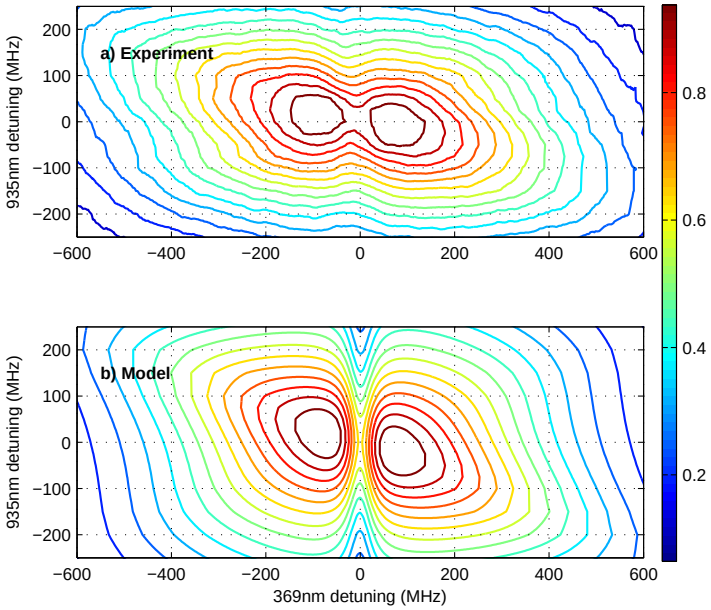

Fig. 4. Contour plots showing the topology of the coupled resonance signal from the lock-in amplifier referenced to the 935nm laser as a function of the 369nm and 935nm laser detunings. (a) The experimental results obtained by locking the 935nm laser to a wavelength meter and scanning the 369nm laser. (b) The topology predicted by a rate equation model incorporating strong velocity changing collisions.

probe beam. To capture all the qualitative features of the measurement, we incorporate strong velocity changing collision (VCC) into the model [12]. In the HCDL discharge, ytterbium ions will predominantly experience collisions with the neon buffer gas for which $m_{Yb}/m_{Ne} = 8.7$, m_{Yb} being the mass of ytterbium ions, and m_{Ne} the mass of neon atoms. In the several hundred Pascal neon background pressure, an ytterbium ion will undergo several collisions during the time it takes for it to undergo the scattering cycle ${}^2S_{1/2} \longrightarrow {}^2D_{3/2} \longrightarrow {}^2S_{1/2}$. As a result, the velocity of the ytterbium ion at the beginning of the cycle will be uncorrelated to the velocity at the end of the cycle, which makes a strong VCC model appropriate. For atoms moving with velocity v, the number densities in the ${}^2S_{1/2}$, ${}^2P_{1/2}$, ${}^2D_{3/2}$ and ${}^3D[3/2]_{1/2}$ levels are denoted by n_1, n_2, n_3 and n_4 respectively. The rate equations for the four-level system are given by

$$\frac{dn_1(v)}{dt} = \frac{1}{\tau_2}\left(\frac{I_{1Pump}}{2I_{s1}(\omega_1,v)} + \frac{I_{1Probe}}{2I_{s1}(\omega_1,-v)}\right)(-n_1(v)+n_2(v)) + b_{21}\frac{n_2(v)}{\tau_2} + b_{41}\frac{n_4(v)}{\tau_4} + R_{31}n_3(v) - R_{13}n_1(v) + R_c\left[n_1(v) - G(v)\int n_1(v')dv'\right] \quad (1)$$

$$\frac{dn_2(v)}{dt} = \frac{1}{\tau_2}\left(\frac{I_{1Pump}}{2I_{s1}(\omega_1,v)} + \frac{I_{1Probe}}{2I_{s1}(\omega_1,-v)}\right)(n_1(v)-n_2(v)) - \frac{n_2(v)}{\tau_2} +$$

#217611 - $15.00 USD Received 23 Jul 2014; revised 29 Aug 2014; accepted 1 Sep 2014; published 7 Oct 2014

$$R_c\left[n_2(v)-G(v)\int n_2(v')dv'\right] \tag{2}$$

$$\frac{dn_3(v)}{dt}=\frac{1}{\tau_4}\left(\frac{I_{2Pump}}{2I_{s2}(\omega_2,v)}\right)(-n_3(v)+n_4(v))+b_{43}\frac{n_4(v)}{\tau_4}+$$
$$b_{23}\frac{n_2(v)}{\tau_2}-R_{31}n_3(v)+R_{13}n_1(v)+R_c\left[n_3(v)-G(v)\int n_3(v')dv'\right] \tag{3}$$

$$\frac{dn_4}{dt}=\frac{1}{\tau_4}\left(\frac{I_{2Pump}}{2I_{s2}(\omega_2,v)}\right)(n_3(v)-n_4(v))-\frac{n_4(v)}{\tau_4}+$$
$$R_c\left[n_4(v)-G(v)\int n_4(v')dv'\right]. \tag{4}$$

The terms in square brackets describe redistribution of velocities in a given level due to strong velocity changing collisions [12], [13]. R_c is the strong collision rate constant. The detailed population balance for the number densities is

$$n_1(v)+n_2(v)+n_3(v)+n_4(v)=G(v)N, \tag{5}$$

where $G(v)$ is the Maxwell-Boltzmann distribution at temperature T. The total number density $N=N_1+N_2+N_3+N_4$. For a given level i, $N_i=\int n_i(v')dv'$. In the rate equations, the angular frequencies of the 369nm and 935nm radiation are ω_1 and ω_2 respectively, and the lifetimes of states 2 and 4 are τ_2 and τ_4 respectively. R_{13} and R_{31} are rate constants for non-radiative decay population transfer between levels 1 and 3. This is necessary to maintain a nonzero steady state population in the $^2D_{3/2}$ state in the absence of laser fields. Such a background population is observed to be present in HCDLs using optogalvanic spectroscopy [9]. The intensity of the 369nm pump and probe beams are I_{1Pump} and I_{1Probe} respectively, while the intensity of the 935nm laser is I_{2Pump}. Note that the pump beams from both lasers propagate collinearly in the same direction, counter to the propagation direction of the 369nm probe beam. The frequency dependent saturation intensity is given by [14]

$$I_s(\omega,v)=\frac{\hbar\omega}{2\tau\sigma_0 g(\omega,v)}, \tag{6}$$

where $\sigma_0=3\lambda_0^2/2\pi$ is the on resonance absorption cross section, λ_0 the on resonance wavelength related to the wave vector through $k=2\pi/\lambda$, and $g(\omega,v)$ is the Lorentzian lineshape function

$$g(\omega,v)=(\Gamma/2)^2/((\Gamma/2)^2+(\omega-\omega_0-vk)^2). \tag{7}$$

The angular homogenous widths of the 369nm and 935nm transitions are denoted Γ_1 and Γ_2 respectively. At a given ω_1 ,ω_2, Eqs. (1) to (4) are solved numerically to find the populations at each velocity. For an optically thin sample, the change in intensity of the probe beam is given by the rate at which 369nm photons are scattered out of the beam per unit area. This is

$$\Delta I_{probe}(\omega_1,\omega_2,v)=\frac{n_2}{\tau_2}\hbar\omega\Delta z. \tag{8}$$

This intensity is integrated over all velocities to obtain the frequency dependent change in intensity $\Delta I(\omega_1,\omega_2)$. The output of the lock-in detector, referenced to the 935nm intensity modulation frequency, will then be $I_C(\omega)=\Delta I(\omega_1,\omega_2)$-$\Delta I(\omega_1,\omega_2)|_{\text{935nm laser off}}$, Where the latter term is obtained from Eqs. (1) to (4) using $I_{2Pump}=0$. In the model we use the same laser beam intensities as those used experimentally to obtain Fig. 3, and the following quantities were used as fitting parameters: the homogenous width of the $^2\mathrm{D}_{3/2}\rightarrow{}^3\mathrm{D}[3/2]_{1/2}$ transition (Γ_2), the rate

#217611 - $15.00 USD Received 23 Jul 2014; revised 29 Aug 2014; accepted 1 Sep 2014; published 7 Oct 2014

of non-radiative decay from $^2D_{3/2} \rightarrow ^2S_{1/2}$ (R_{31}), and the rate of non-radiative population of the $^2D_{3/2}$ from the ground state (R_{13}), and the strong velocity collision rate (R_c). The Nealder-Mead algorithm was used to find the optimal value of these parameters to minimize the sum of the squared differences between the experimental data shown in Fig. 4(a) and the model. The optimized values of the fitting parameters are $\Gamma_2 = 2\pi \times 0.48$MHz, $R_{13} = 2.0 \times 10^4 s^{-1}$ and $R_{31} = 8.9 \times 10^6 s^{-1}$. The strong collision rate constant is $R_c = 9.5 \times 10^6 s^{-1}$. This value of R_c is consistent with the expected collision rate for the buffer gas pressure in our HCDL.

Notice in Fig. 4 that the model in Fig. 4(b) successfully predicts many of the qualitative aspects of the experimental results in Fig. 4(a), including fine features like the shallow valleys that we consistently observe along the axis of zero 935nm detuning on the outside slopes of the two dominant peaks. The model clearly explains the appearance of the double resonance signal in Fig. 3, although it somewhat overestimates the depth of the central dip.

3. Laser frequency stabilization

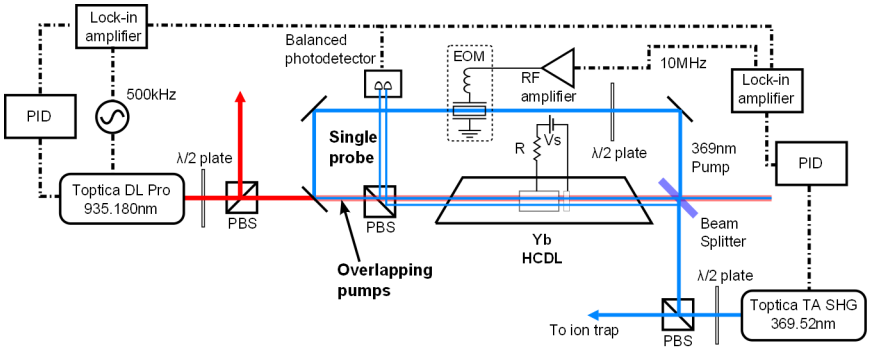

Fig. 5. Experimental setup for performing laser frequency stabilization using CORELL. An EOM is used to phase modulate the pump beam of the 369nm laser. The 935nm laser is current modulated.

Finally, we exploit the coupled resonance signal to simultaneously frequency stabilize both our lasers. The experimental setup for this is shown in Fig. 5. In this instance the 369nm pump beam power before the HCDL was measured to be 0.81mW. The 369nm probe beam power was 0.11mW, and 10mW of 935nm light was used. Beam radii at the lamp center were 0.4mm. Proportional-integral-derivative (PID) controllers are used as loop filters. Observe again that the photodiode signal is used as the input to both lock-in amplifiers and that the two lock-in amplifiers are referenced to different modulation frequencies. In order to generate a derivative signal for locking the 369nm laser to the $^2S_{1/2} \rightarrow ^2P_{1/2}$ transition of $^{174}Yb^+$, we now resort to modulation transfer spectroscopy [15–17]. To that end an electro-optic modulator (EOM) replaces the chopper wheel in Fig. 2, and is used to phase modulate the 369nm pump beam at 10MHz with a modulation depth of 4.3. The 369nm error signal for $^{174}Yb^+$is shown in Fig. 6(a). The frequency axis was calibrated using a Fabry-Perot interferometer with a free spectral range of 1.5GHz. The slope of the error signal is -44.8mV/MHz. Fig. 6(b) shows the locked error signal over a period of 1000s. The slope of the error signal was used to estimate the frequency deviation from the locked error signal voltage. The standard deviation of the error signal from the lock point was calculated to be $\sigma = 0.44$MHz which is sufficient for cooling ytterbium ions. Once the 369nm laser is locked to the $^{174}Yb^+$ line, the 935nm laser is scanned

#217611 - $15.00 USD Received 23 Jul 2014; revised 29 Aug 2014; accepted 1 Sep 2014; published 7 Oct 2014

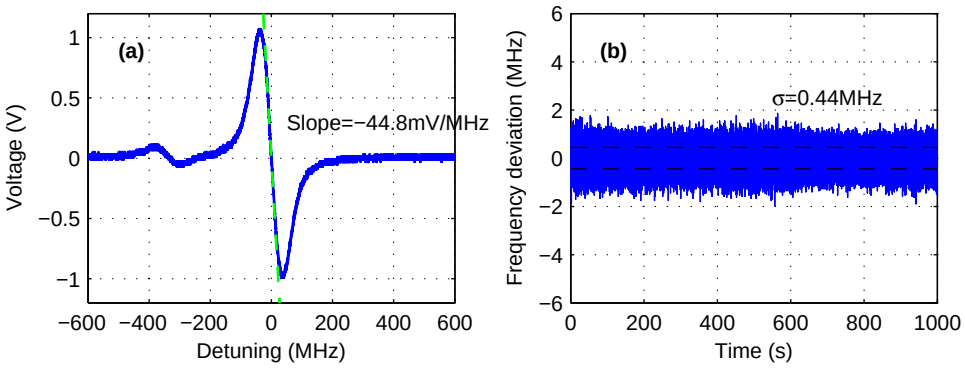

Fig. 6. (a) Experimental 369nm modulation transfer spectroscopy error signal for $^{174}Yb^{+}$ in solid blue. The dashed green line shows the slope of the error signal at the zero crossing point. A lock in time constant of 0.5ms and scaling of 50V/Vrms were used. In (b), the blue curve shows the experimental locked error signal over a period of 1000s. The dashed black lines indicate one standard deviation above and below the lock point.

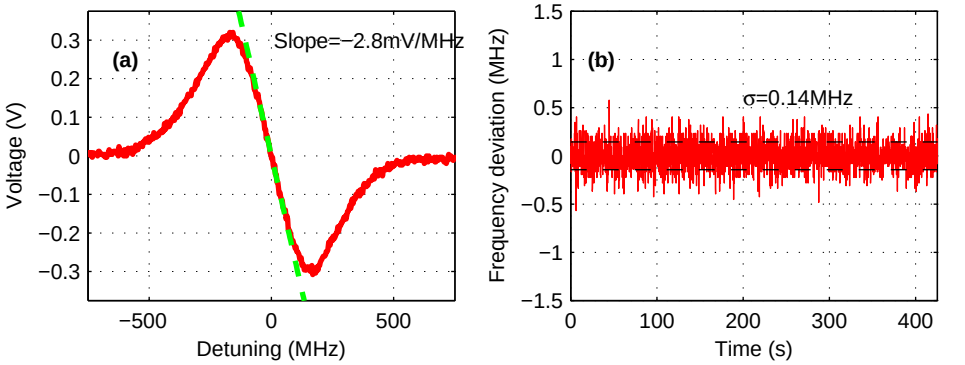

Fig. 7. (a) Experimental 935nm CORELL error signal for the $^{174}Yb^{+}$ $^{2}D_{3/2} \rightarrow {}^{3}D[3/2]_{1/2}$ transition in solid red. The dashed green line shows the slope of the error signal at the zero crossing point. The 369nm laser is locked to the resonance center. In (b), the red curve shows the experimental locked error signal over a period of 450s. The dashed black lines indicate one standard deviation above and below the lock point. A lock in time constant of 221ms was used with a scaling of 50V/Vrms.

across the $^{2}D_{3/2} \rightarrow {}^{3}D[3/2]_{1/2}$ of the same isotope. Current modulation of the 935nm beam at 500 kHz with a modulation depth of 840, combined with lock-in detection, produces a high signal-to-noise ratio derivative signal (the CORELL signal). Fig. 7(a) shows this signal, which can be thought of as the derivative of a vertical cut of the surface shown in Fig. 4, at zero detuning of the 369nm laser. Note that while the weak 369nm reference beam is not necessary, it helps to reduce noise in the 935nm CORELL signal. The slope of the zero crossing point was measured to be -2.8mV/MHz. With a lock in time constant of 221ms, the 935nm laser was locked to the CORELL signal for 450s. The locked error signal is shown in Fig. 7(b). The standard deviation in the signal is $\sigma = 0.14$MHz is more than sufficient for metastable state repumping. Note that the data in Fig. 6(b) and and Fig. 7(b) was taken simultaneously. The CORELL signal provides a long term frequency reference and the closed loop system is able

#217611 - $15.00 USD Received 23 Jul 2014; revised 29 Aug 2014; accepted 1 Sep 2014; published 7 Oct 2014

to reject disturbances imposed by changing environmental conditions. The long term stabilities obtained here with both lasers locked approach the fundamental short time (few microsecond) bandwidth of the diode lasers, which is likely limited by mechanical vibrations. Observe that the frequency deviation of the 369nm laser is larger than that of the 935nm laser despite a significantly steeper slope in the error signal of the 369nm laser. However, when scaled by the ratio of wavelengths one finds that the performances are comparable.

4. Conclusion

We have presented a method for simultaneously locking both a UV and IR laser to coupled resonances in a single spectroscopic sample and applied the method for locking different lasers to the $^2S_{1/2} \rightarrow ^2P_{1/2}$ and $^2D_{3/2} \rightarrow {}^3D[3/2]_{1/2}$ transitions of $^{174}Yb^+$. Separate but coupled spectroscopic signals suitable for laser locking can be obtained for all of the lasers by observing only a single probe beam from one of the lasers. The separate signals are distilled from the single probe by modulating each laser at a different frequency and using lock-in detection. This method provides a signal to stabilize the 935 nm laser which in isolation exhibits only weak absorption due to an efficient Raman decay channel to the $^2S_{1/2}$ ground state. The stabilized linewidths of both lasers are more than an order of magnitude narrower than the natural linewidths of the relevant transitions, making them well suited for the purposes of ion cooling and metastable state repumping. A rate equation model incorporating strong velocity changing collisions describes the coupled resonance spectroscopy features that are used for laser stabilization. Our technique should be readily applicable to other ion or neutral atom systems with similarly coupled cooling and repumping transitions. Although we have motivated CORELL mainly for atom cooling applications, it should be useful in other atomic and molecular physics experiments like high resolution spectroscopy.

Acknowledgments

This work is supported by the National Research Foundation of South Africa. Grant numbers 74437 and 82416.

#217611 - $15.00 USD Received 23 Jul 2014; revised 29 Aug 2014; accepted 1 Sep 2014; published 7 Oct 2014